

Engineering the Unique 2D Mat of Graphene to Achieve Graphene-TiO₂ Nanocomposite for Photocatalytic Selective Transformation: What Advantage does Graphene Have over Its Forebear Carbon Nanotube?

Yanhui Zhang,^{†,‡} Zi-Rong Tang,[†] Xianzhi Fu,^{†,‡} and Yi-Jun Xu^{†,‡,*}

[†]College of Chemistry and Chemical Engineering, Fuzhou University, Fuzhou 350108, People's Republic of China, and [‡]State Key Laboratory Breeding Base of Photocatalysis and College of Chemistry and Chemical Engineering, Fuzhou University, Fuzhou 350002, People's Republic of China

Recent years have witnessed a cornucopia toward the synthetic fabrication of graphene-based nanocomposites and their potential applications in a myriad of fields, for example, nanoelectronics, biosensors, intercalation materials, supercapacitors, drug delivery, polymer composites, and catalysis.^{1–11} In particular, the unique and outstanding properties of graphene, including excellent electron conductivity and high transparency, have spurred increasing interest to synthesize the graphene (GR)-semiconductor nanocomposites as photocatalysts for degradation of pollutants (dyes, bacteria, and volatile organic pollutant) as well as water splitting to H₂.^{12–21} Notably, research works, as reported in literature, are inclined to overemphasize the enhanced photocatalytic activity of GR-semiconductor nanocomposites resulted from the addition of GR. In fact, this case is similar to that for its forbear carbon nanotubes (CNT)-semiconductor photocatalysts.^{22–27} But a thoughtful and inevitable comparison between GR- and CNT-semiconductors as photocatalysts is often neglected.^{12–21} This situation may give incomplete or exaggerated information on the contribution role of GR to enhance the semiconductor photocatalytic activity, as compared to its carbon allotrope, CNT.^{12,13} Therefore, our knowledge regarding the specific advantage of GR over its forbear CNT on how to design or fabricate efficient GR-semiconductor nanocomposites and understand the origin of their enhanced photocatalytic performance is far from

ABSTRACT Increasing interest has been devoted to synthesizing graphene (GR)-semiconductor nanocomposites as photocatalysts for potential applications, which is very similar to its forbear carbon nanotube (CNT)-semiconductor photocatalysts. Unfortunately, a thoughtful and inevitable comparison between GR- and CNT-semiconductors as photocatalysts is often neglected in literature. This situation may give incomplete or exaggerated information on the contribution role of GR to enhance the semiconductor photocatalytic activity, as compared to CNT. Thus, our knowledge regarding the specific advantage of GR over CNT on how to design more efficient GR-semiconductor nanocomposites and understanding the origin of their enhanced photocatalytic performance is far from satisfactory. By taking the TiO₂ semiconductor as an example, we conceptually demonstrate how to synthesize a more efficient GR-TiO₂ nanocomposite as a visible light photocatalyst toward selective oxidation of alcohols under mild conditions. Comparison between GR-TiO₂ and CNT-TiO₂ discloses the prominent advantage of GR over CNT on both controlling the morphology of GR-TiO₂ nanocomposite and enhancing the photocatalytic activity of TiO₂. This work clearly highlights the importance and necessity for a comparison investigation between GR- and CNT-semiconductors as photocatalysts, which will promote our in-depth fundamental understanding on the analogy and difference between GR and CNT on controlling the morphology of GR (or CNT)-semiconductor nanocomposites and enhancing the photocatalytic performance. Therefore, we appeal the photocatalysis community to pay attention to this respect rather than separately imposing hype on the mirage of GR in much the same way as its carbon forebears, which could significantly advance our rational fabrication of smart GR-semiconductor nanocomposites for artificial photosynthesis.

KEYWORDS: graphene · TiO₂ · nanocomposite · visible light photocatalysis · selective oxidation

satisfactory. Furthermore, so far, the rational synthesis of highly active GR-semiconductor nanocomposites in an appropriate fashion as visible light photocatalysts for selective organic transformations under mild conditions is still unavailable.

In principle, in order to achieve an efficient GR-semiconductor photocatalyst, one should consider how to adequately harness

* Address correspondence to yjxu@fzu.edu.cn.

Received for review June 24, 2011 and accepted August 26, 2011.

Published online August 26, 2011 10.1021/nn202519j

© 2011 American Chemical Society

the unique two-dimensional (2D) “mat” structure and extraordinary electron-transport property of GR. An ideally possible route is to cover the individual 2D sheet of GR with semiconductor ingredients fully and intimately, by which we can maximize the excellent electron conductivity of GR, owing to the sufficient interfacial contact between GR and semiconductor. As a result, the lifetime of charge carriers photogenerated from semiconductors upon light irradiation could be prolonged much more effectively as compared to the simply random integration of GR and semiconductors for which the interfacial contact between titanium dioxide (TiO₂) and GR sheet is rather insufficient.^{12,13}

Herein, using the mostly studied TiO₂ semiconductor as an example, we demonstrate the synthesis of GR-TiO₂ nanocomposites by interfacial engineering of the 2D mat of GR with TiF₄ as precursor in an aqueous phase, and their application as an active visible light photocatalyst for selective oxidation of alcohols to corresponding aldehydes, a key transformation for the synthesis of fine chemicals,^{28–30} under ambient conditions. In addition, the CNT-TiO₂ nanocomposites have also been prepared using the similar approach. A careful comparison study between GR-TiO₂ photocatalysts and their analogues CNT-TiO₂ discloses the significant effect of preparative methods on the microstructure of GR-TiO₂ nanocomposite and, hence, its photocatalytic performance. With the current synthesis approach, the superior and easily accessible “structure-directing” role of graphene oxide (GO) (the precursor of GR) in an aqueous phase is able to be utilized sufficiently. As a result, the interfacial contact between the GR sheet and TiO₂ is rather sufficient for the as-prepared GR-TiO₂ nanocomposite, which gives rise to the more effective separation of photogenerated electron–hole pairs and in turn leads to the significantly enhanced photocatalytic performance of GR-TiO₂ toward selective oxidation of alcohols to aldehydes under the irradiation of visible light.

Notably, our research work is the first time, by a systematic comparison study between GR-TiO₂ photocatalysts and their analogues CNT-TiO₂, to demonstrate conceptually on how to synthesize a more efficient GR-semiconductor visible light photocatalyst for selective organic transformations. The results particularly highlight the key importance and necessity to perform a comparison study between GR- and CNT-semiconductors as photocatalysts for a given target application, because it will promote our in-depth fundamental understanding on the analogy and difference between GR and CNT on how to control the morphology of GR (or CNT)-semiconductor nanocomposites and enhance the photocatalytic performance. Unfortunately, such a comparison is often neglected so far in literature.^{12–21} Therefore, in this sense, we appeal the photocatalysis community to pay attention to this respect rather than separately imposing hype on the

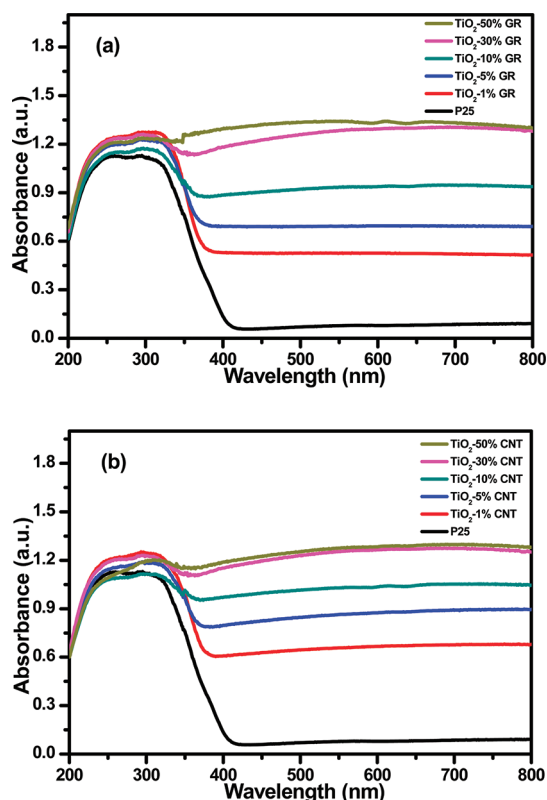


Figure 1. The UV–vis DRS of GR-TiO₂ nanocomposites (a) and their analogues CNT-TiO₂ nanocomposites (b).

miracle of GR in much the same way as its carbon forebears,^{31,32} which could significantly advance our rational fabrication of smart GR-semiconductor nanocomposites for artificial photosynthesis.

RESULTS AND DISCUSSION

The GR-TiO₂ nanocomposites with different weight addition ratios (1, 5, 10, 30, and 50%) of GR have been prepared based on a two-step process in a solution phase. The first step is to load the semiconductor TiO₂ ingredient onto the 2D sheet of GO by the hydrolysis process of TiF₄ in a well-dispersed GO aqueous solution at low temperature. Subsequently, insulating GO is transformed to electron conducting GR by a hydrothermal treatment in an ethanol–water solution,^{12,13} by which the GR-TiO₂ nanocomposites can be obtained. Figure 1a displays the UV–vis diffuse reflectance spectra (DRS) of the as-obtained GR-TiO₂ nanocomposites. For comparison purpose, their analogues CNT-TiO₂ nanocomposites prepared by the same approach are also shown in Figure 1b. As can be seen clearly, the addition of GR or CNT induces the increased light absorption intensity in both the UV and visible light regions, as compared to the bare TiO₂. Furthermore, a qualitative red shift to higher wavelength is observed in the absorption edge of both GR-TiO₂ and CNT-TiO₂ nanocomposites. Therefore, the introduction of GR or CNT into the matrix of GR-TiO₂

or CNT-TiO₂ is able to effectively promote the visible light response of the nanocomposites of GR-TiO₂ and CNT-TiO₂, which can be attributed to electronic interactions between GR or CNT and TiO₂.^{12,13} Such an extended optical absorption has also been observed in previous research works regarding GR- or CNT-semiconductor photocatalysts for degradation of organic pollutants.^{12–27}

Figure 2 shows the XRD patterns of the as-prepared GR-TiO₂ and CNT-TiO₂ nanocomposites, respectively. It is clear to see that the GR-TiO₂ nanocomposites with different weight addition ratios of GR have similar XRD patterns. The peaks located at 25.3, 37.8, 48.0, 53.9, 55.1, 62.7, 68.8, 70.3, and 75.0° can be indexed to (101), (004), (200), (105), (211), (204), (116), (220), and (215) crystal planes of anatase TiO₂. No typical diffraction peaks of GR are observed in the GR-TiO₂ nanocomposites. This is because the main characteristic peak of GR at 25.0° is overlapped with the (101) peak of anatase TiO₂. Regarding the CNT-TiO₂ nanocomposites with the weight addition ratios of CNT lower than 30%, the XRD patterns are very similar to that for GR-TiO₂. When the weight addition ratios of CNT reach 30 and 50%, the typical peak of CNT at 26.2° can be clearly identified in the XRD patterns.

Our initial experiments on photocatalytic selective oxidation of alcohols begin with the activity testing on benzyl alcohol under visible light irradiation. As shown in Figure 3a, it is crucial to control the addition ratios of GR in order to achieve an optimal synergy interaction between GR and TiO₂ for selective oxidation of alcohols. The nanocomposite of TiO₂-5% GR exhibits the best visible light photocatalytic performance toward selective oxidation of benzyl alcohol to benzyl aldehyde. Under the irradiation of 4 h, the 100% selectivity along with 30% conversion is reached. For comparison purpose, the photocatalytic performance of their analogues CNT-TiO₂ nanocomposites prepared by the same approach is also performed, as shown in Figure 3b. Similarly, TiO₂-5% CNT shows the best photocatalytic performance. Nevertheless, the conversion is only 6% along with 97% selectivity. This manifests that the TiO₂-5% GR nanocomposite is over five times more active than its analogue TiO₂-5% CNT. Time–online activity testing further corroborates the superior advantage of as-prepared GR-TiO₂ over CNT-TiO₂ as a visible light photocatalyst for selective oxidation of alcohol to corresponding aldehyde, as shown in Figure 3c.

However, if we change to prepare GR-TiO₂ by a simply random integration of solid TiO₂ particles (taking P25 as example) with GR,^{12,13} then the scenario of activity enhancement will be remarkably different under the same reaction conditions. As shown in Figure S1 (Supporting Information), the conversion of benzyl alcohol is 14% along with 91% selectivity over the optimal photocatalyst of P25-1% GR. Whereas, over

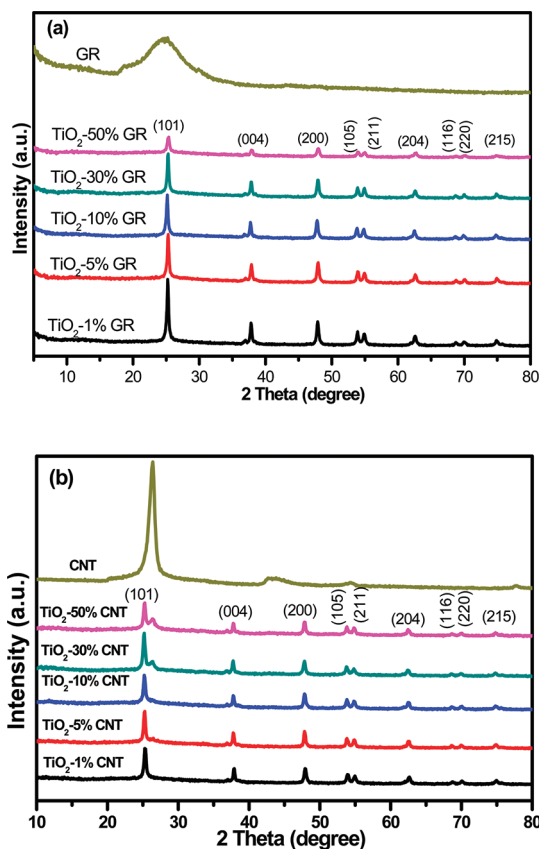


Figure 2. The XRD patterns of GR-TiO₂ nanocomposites (a) and their analogues CNT-TiO₂ nanocomposites (b).

its analogue P25-1% CNT, 11% conversion and 90% selectivity are obtained. This means a slight increase of photocatalytic activity by 22% for P25-1% GR, as compared to P25-1% CNT, based on the yield of benzyl aldehyde. In such a case, the well-known unique properties of GR on enhancement of TiO₂ photocatalytic activity cannot be fully reflected as compared to its carbon allotrope CNT. We have also performed the comparison activity testing on selective oxidation of other benzylic and allylic alcohols to corresponding aldehydes under visible light irradiation (Figure S2, Supporting Information,) over TiO₂-5% GR, TiO₂-5% CNT, P25-1% GR, and P25-1% CNT, for which similar activity trend is also observed. Thus, under this circumstance, the statement on claiming the unique and superior role of GR over CNT on improving the semiconductor photocatalytic activity is exaggerated.^{12,13} Our current experiments clearly suggest that the preparation methods play a very important role in affecting the photocatalytic performance of GR-TiO₂ nanocomposite.

“Structure dictates function” is the basic concept in chemistry, which has been widely recognized by the well-established morphology-dependent photocatalytic activity.^{33–36} Therefore, we infer that the microscopic morphology of GR-TiO₂ prepared by the current approach should be distinctly different from CNT-TiO₂

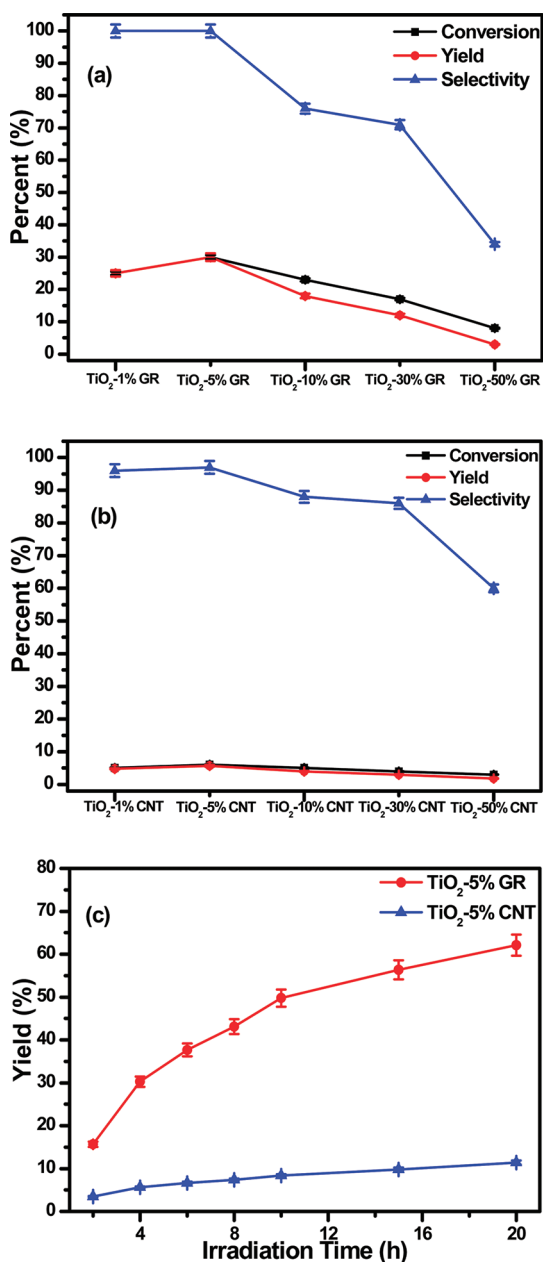


Figure 3. Selective oxidation of benzyl alcohol to benzaldehyde over the nanocomposites of GR-TiO₂ (a) and CNT-TiO₂ (b) with different weight addition ratios of GR and CNT, respectively, under visible light irradiation of 4 h; time-online profile of yield of benzyl aldehyde over the optimal TiO₂-5% GR and TiO₂-5% CNT nanocomposites (c).

and that prepared by the simply random integration of TiO₂ nanoparticles and GR sheet.^{12,13} This is directly evidenced by the scanning electron microscopy (SEM) and transmission electron microscopy (TEM) analysis. Figure 4a, c, and d shows the typical SEM and TEM images of TiO₂-5% GR nanocomposite, respectively. It is clear that the GR sheet and semiconductor TiO₂ ingredients have been integrated by way of an intimate interfacial contact. The stacking GR layers can also be identified in the edge area of TiO₂-5% GR, as shown in Figure 4e. However, with the current synthesis

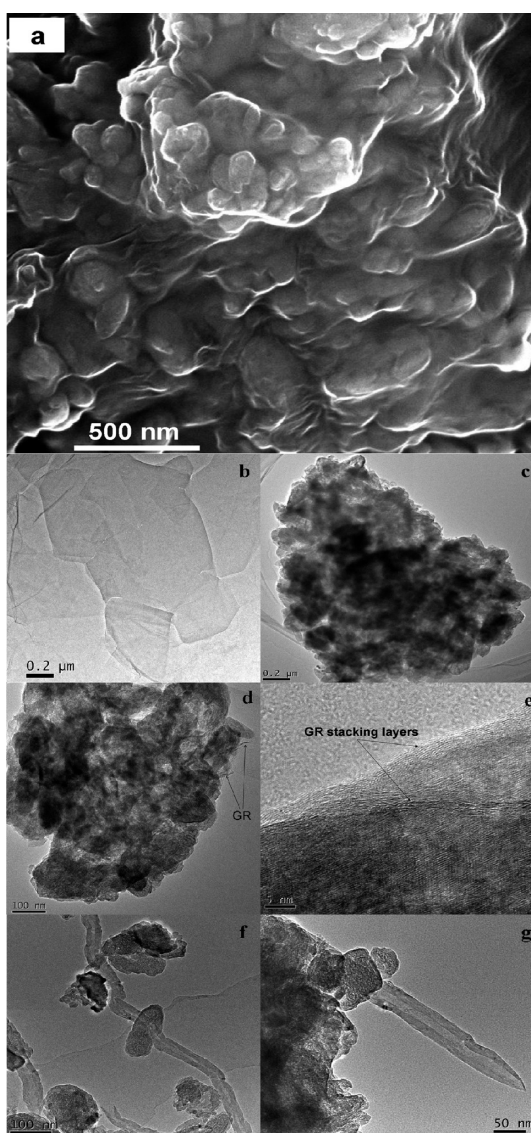


Figure 4. SEM image of TiO₂-5% GR (a); and TEM images of GR (b), TiO₂-5% GR (c and d), TiO₂-5% CNT (f and g), and HRTEM image of TiO₂-5% GR (e).

approach, the interfacial integration of CNT and TiO₂ is ineffective, as proved by the TEM images in Figure 4f and g. This demonstrates the superior and easily accessible structure-directing role of GO (the precursor of GR) over CNT as a “solution processable surfactant”.³⁷ Notably, such an intimate complexation of TiO₂ and GR cannot be obtained by the simply random integration of solid TiO₂ nanoparticles and GR sheet.^{12,13,18,19} The significant drawback of this preparation method is attributed to the fact that: (i) complexation of solid TiO₂ nanoparticles with GO can not effectively utilize the “structure-directing” role of GO, owing to its unique 2D structure with abundant oxygen-containing functional groups on the basal plane and edge that provide reactive sites to interact with organic/inorganic systems;^{37,38} and (ii) thus, a simple integration of solid TiO₂ nanoparticles with GR is not able to give a

maximum interfacial contact between TiO_2 and GR, resulting in insufficient utilization of excellent electron conductivity of GR and insufficient antirecombination of electron–hole pairs photogenerated from TiO_2 upon light irradiation. When water-soluble inorganic salt of TiF_4 , instead of solid TiO_2 particles, is used as precursor of TiO_2 , it can sufficiently interact with the functional groups of well-dispersed GO in an aqueous phase, thereby leading to the intimate integration of the GR sheet and TiO_2 ingredients, as evidenced by the SEM and TEM analysis. In this case, the excellent electron conductivity of GR is able to be utilized efficiently, thus enhancing the lifetime of photogenerated electron–hole pairs more effectively. This in turn leads to the observation of much higher photocatalytic activity of GR- TiO_2 toward selective oxidation of alcohols.

To further understand the significant role of sufficient and intimate interfacial contact between GR sheet and TiO_2 on enhancing the lifetime of electron–hole pairs and promoting photocatalytic activity, the photoelectrochemical experiments are performed. Figure 5 displays the photocurrent transient response for TiO_2 -5% GR, TiO_2 -5% CNT, P25-1% GR, P25-1% CNT, and bare P25 electrodes, under visible light irradiation. As is clearly seen, TiO_2 -5% GR prepared by the current approach has the highest photocurrent density as compared to other samples; moreover, the photocurrent is quite stable, i.e., no obvious photocurrent decay is observed. This indicates that the transport of photogenerated electrons to GR is markedly effective. Thus, the inhibition degree of photogenerated electron–hole pairs recombination is the most pronounced for TiO_2 -5% GR. In contrast, the photocurrent density for other samples is lower. In addition, the significant photocurrent decay is observed with the increased switch-on and -off cycles, indicating the obvious recombination process of photogenerated electron–hole pairs is occurring. After the equilibration of competitive separation and recombination of photogenerated electron–hole pairs, the photocurrent reaches a relatively constant value. The higher and more stable photocurrent for TiO_2 -5% GR, prepared by the current approach, is in agreement with its highest photocatalytic activity toward selective oxidation of alcohols under visible light irradiation and highlights the key importance to integrate GR sheet and semiconductor ingredients fully and intimately on prolonging the lifetime of photogenerated electron–hole pairs.

The results of electron spin resonance (ESR) experiments, as shown in Figure 6, further support the viewpoint that a sufficient and intimate interfacial contact between GR sheet and TiO_2 can effectively promote the separation of photogenerated electron–hole pairs. For TiO_2 -5% GR under visible light irradiation, a stable and higher superoxide radical species intensity can be reached with the increased irradiation time (Figure 6a),

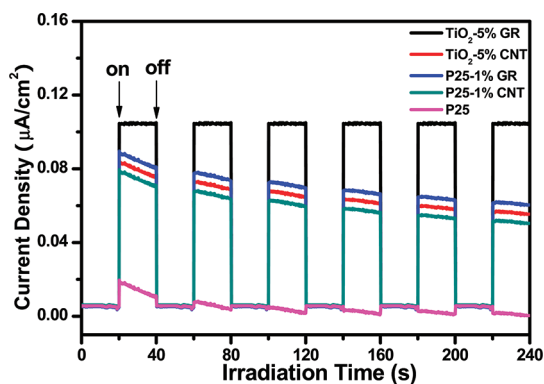


Figure 5. Photocurrent transient response of the samples TiO_2 -5% GR, TiO_2 -5% CNT, P25-1% GR, P25-1% CNT, and bare P25 in a 0.2 M of Na_2SO_4 aqueous solution under visible light irradiation.

as compared with its analogue TiO_2 -5% CNT (Figure 6b). In analogy, with regard to P25-1% GR and P25-1% CNT prepared by the simple integration of solid P25 particles with GR sheet, a decay and lower superoxide radical species intensity is also observed, as shown in Figure 6c and d. These findings seem nicely consistent with the results of stable and higher photocurrent generated for TiO_2 -5% GR upon visible light irradiation. The other observation from ESR analysis is that strong and nonselective hydroxyl radical species are not detected, which has also been observed in previous research works.^{29,39}

To ensure that the surface area is not the major factor causing such an obvious photoactivity improvement for TiO_2 -5% GR as compared to P25-1% GR, we have performed the Brunauer–Emmett–Teller (BET) specific surface area analysis of these samples (Table S1, Supporting Information). The surface area of TiO_2 -5% GR is determined to be *ca.* $69 \text{ m}^2 \cdot \text{g}^{-1}$, which is very similar to *ca.* $65 \text{ m}^2 \cdot \text{g}^{-1}$ for P25-1% GR. In addition, it should be noted (Table S1, Supporting Information) that the continued increase in surface area provided by the more weight addition of GR does not lead to the improvement in photoactivity. Indeed, the total pore volume and porosity between TiO_2 -5% GR and P25-1% GR are almost identical (Figures S3 and S4, Supporting Information). Thus, these photocatalysts should have similar adsorption capacity toward alcohols, which is faithfully confirmed by the data in Figure 7. All of these results strongly suggest that the surface area and porosity difference between TiO_2 -5% GR and P25-1% GR is unlikely the major factor that accounts for the large discrepancy between their photoactivity difference. Similar issue has also been observed for photocatalytic reduction of CO_2 over P25-GR nanocomposites.⁴⁰ Namely, the enhanced lifetime of photogenerated electron–hole pairs, instead of the increased surface area and porosity difference, is the key to improving the photocatalytic performance of P25-GR nanocomposites.

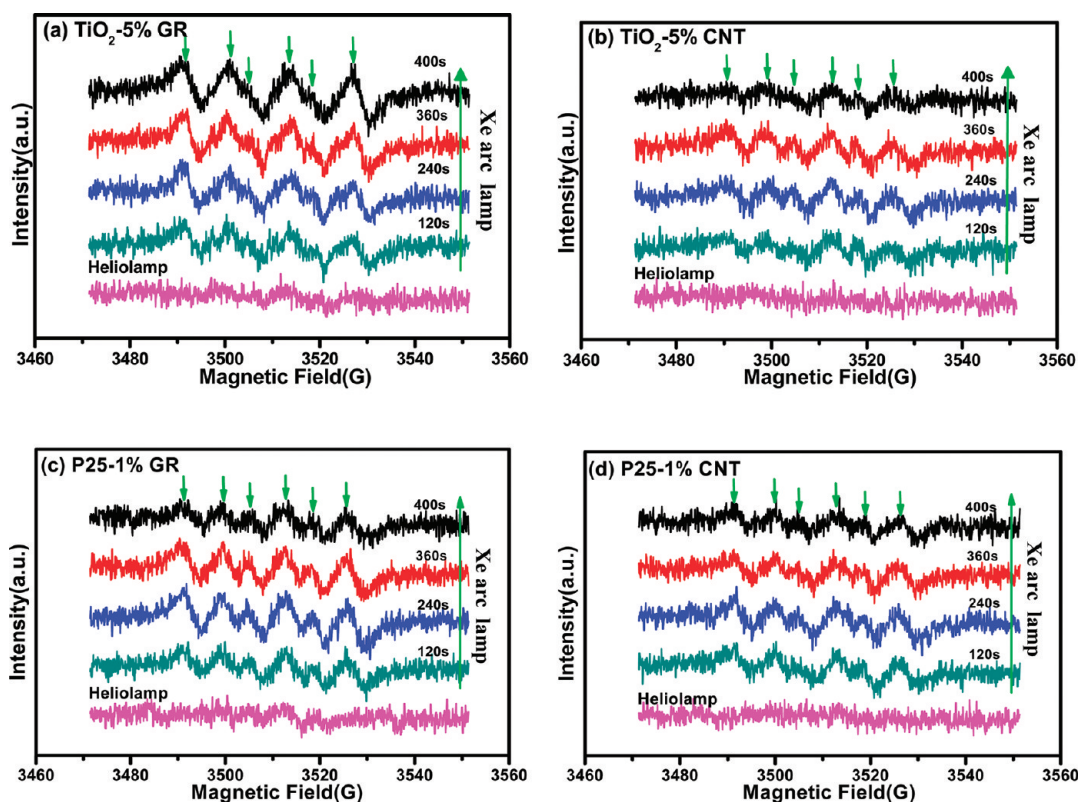


Figure 6. ESR spectra of superoxide radical species trapped by DMPO in TiO₂-5% GR (a), TiO₂-5% CNT (b), P25-1% GR (c), and P25-1% CNT (d) dispersions in the solvent of BTF under visible light irradiation.

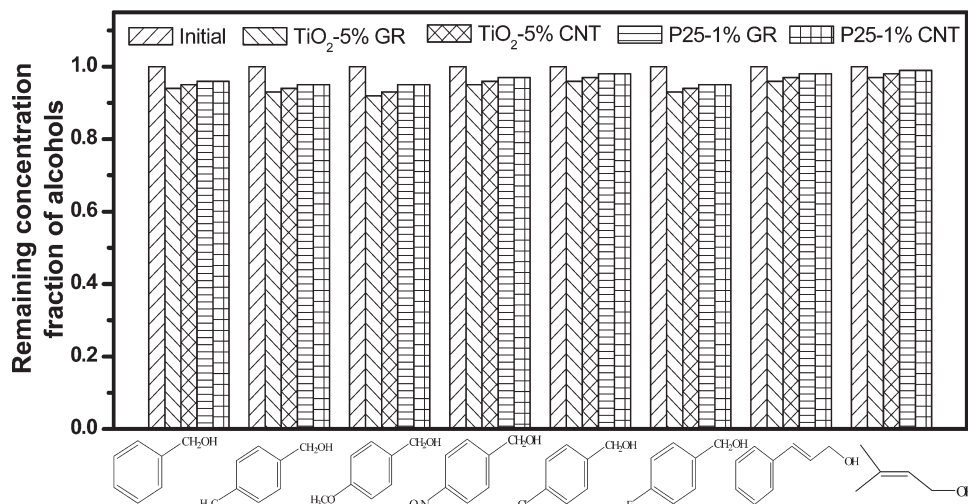


Figure 7. Bar plot showing the remaining concentration fraction of alcohols after the adsorption–desorption equilibrium in the dark over the photocatalysts of TiO₂-5% GR, TiO₂-5% CNT, P25-1% GR, and P25-1% CNT, respectively.

The other issue that should be mentioned is concerning the possible degradation of GR for the nanocomposite of TiO₂-GR during the photocatalytic reaction.^{41,42} In this regard, Raman spectroscopy has been used to examine the changes that occurred in the structure of GR. Typical Raman spectra for the fresh TiO₂-5% GR and used TiO₂-5% GR after visible light degradation for a certain time are shown in Figure 8. Of particular note is the intensity ratio of the D and G bands, I_D/I_G ,

which is a measure of the relative concentration of local defects or disorders (particularly the sp^3 hybridized defects) compared to the sp^2 hybridized graphene domains.^{40–42} It can be seen that, before the solvothermal reduction, the I_D/I_G ratio is 1.11 for TiO₂-5% GO. After the solvothermal reduction, the I_D/I_G ratio is decreased to 1.03, thus indicating more graphitization of TiO₂-5% GR due to the reduction process. In particular, it should be noted that, as compared to that

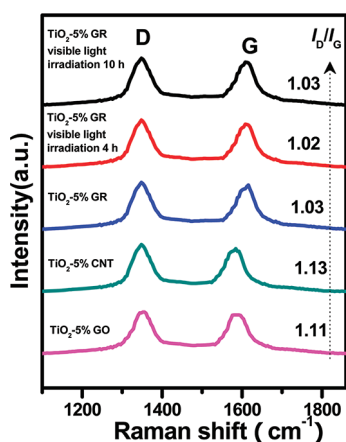


Figure 8. Raman spectra of the photocatalysts of TiO₂-5% GO, TiO₂-5% CNT, TiO₂-5% GR, and TiO₂-5% GR after visible light irradiation for 4 and 10 h in the reaction system, respectively.

for the fresh TiO₂-5% GR, there is no significant change of the I_D/I_G ratio for the used TiO₂-5% GR after visible light irradiation for 4 and 10 h in our photocatalytic reaction system. Hence, it clearly indicates no obvious degradation of GR for our as-prepared TiO₂-5% GR photocatalyst during the reaction, which is also in agreement with the X-ray photoelectron spectroscopy (XPS) results in Figure S9 (Supporting Information).

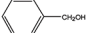
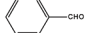
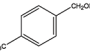
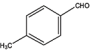
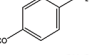
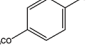
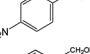
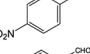
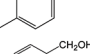
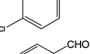
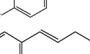
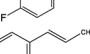
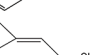
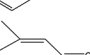


Table 1 shows the photocatalytic performance of TiO₂-5% GR toward selective oxidation of a range of benzylic alcohols with various substituent groups (entries 1–6) and allylic alcohols (entries 7 and 8) to their corresponding aldehydes under the irradiation of visible light. It is clear to see that these alcohols can be transformed to aldehydes with high selectivity (90–100%). The different activity and selectivity suggest that photocatalytic oxidation of alcohols to aldehydes over TiO₂-5% GR might show a stereoselective chemistry. Blank experiments performed in the absence of catalysts and/or visible light show that no conversion of alcohols is observed, confirming the reaction is really driven by a photocatalytic process. A controlled experiment in the presence of nitrogen shows trace conversion of alcohols, thus confirming that oxygen is the primary oxidant that oxofunctionalizes alcohols to aldehydes. In addition, only trace conversion of alcohols is obtained using the bare GR, clearly suggesting TiO₂ is the primary photoactive ingredient in the GR-TiO₂ nanocomposite. Excessive addition of black GR to GR-TiO₂ nanocomposites means the significant amount decrease of primary photoactive ingredient TiO₂¹² and meanwhile lowers the light intensity through the depth of reaction solution. This case is similar to CNT-TiO₂ photocatalysts, for which it has been well recognized that the weight addition ratio of CNT is generally lower than 20%.^{22–27} Therefore, in order to achieve an efficient GR-semiconductor photocatalyst, it is of key importance to control the composition ratio to achieve

an optimal synergy effect between GR and semiconductor and adequately utilize the excellent electron conductivity of GR to increase the lifetime of electron–hole pairs photogenerated from semiconductor.

Thus far, important information based on the present work can be proposed as the following. First, a simply random “hard” integration of solid TiO₂ particles and GR sheets only increases the photocatalytic activity toward selective oxidation of alcohols slightly as compared to its analogue CNT-TiO₂, because the interfacial contact between TiO₂ and GR sheet is relatively weak.^{12,13} Second, the advantages of using water-soluble TiF₄ instead of solid TiO₂ particles to complex with GR sheet are two-fold, which are: First, the structure-directing role of GO with unique 2D structure as a solution processable surfactant is able to be used sufficiently because the well-known abundant oxygen-containing functional groups of GO offer reactive sites to complex with soluble TiF₄.^{37,38} Second, this way of “soft” integration makes the interfacial contact between TiO₂ and GR sheet intimate and sufficient, by which the electron conductivity degree of GR can be maximized leading to the increased lifetime of electron–hole pairs photogenerated from TiO₂. However, such a sufficient interfacial contact cannot be obtained using the same approach for CNT-TiO₂, therefore suggesting the easily accessible advantage of “structure-directing” role of GO over CNT to control the morphology of as-formed GR-TiO₂ nanocomposites. Third, a thoughtful comparison between GR-TiO₂ nanocomposites and their analogues CNT-TiO₂ as photocatalyst is necessary, which can help us understand the specific advantage of GR over CNT on controlling morphology, enhancing photocatalytic activity and, importantly, on how to design more efficient GR-semiconductor photocatalysts for given target applications.

Very recently, Hersam’s group has reported that minimizing graphene defects is able to enhance titania nanocomposite-based photocatalytic reduction of CO₂ for improved solar fuel production.⁴⁰ This work points out that solvent-exfoliated graphene (SEG) with lower defect density has the enhanced electron mobility and a longer electronic mean free path, which enables energetic electrons to diffuse farther from the SEG–P25 interface, thus decreasing the likelihood of their recombination with holes on the TiO₂. Such an improved lifetime of photogenerated electron–hole pairs leads to the significant activity enhancement in photoreduction of CO₂. Importantly, their results suggest that a promising way to improve graphene-TiO₂ photocatalysts may benefit from careful consideration of the electrical properties of the graphene component. Interestingly, our current research work indicates that the photocatalytic performance of graphene-TiO₂ can also be significantly improved by strengthening the interfacial contact between graphene and TiO₂ and, thus, prolonging the photogenerated electron–hole

TABLE 1. Selective Oxidation of a Range of Alcohols over the TiO₂-5% GR Photocatalyst under the Irradiation of Visible Light for 20 h.

Entry	Substrate	Product	Conv.(%)	Yield (%)	Sel.(%)
1			62	62	100
2			70	70	100
3			80	80	100
4			74	73	99
5			45	43	96
6			84	76	91
7			50	46	92
8			41	37	90

pairs lifetime more effectively. The key to achieve this sufficient interfacial contact is to adequately utilize the superior structure-directing role of GO with soluble inorganic salt TiF₄, rather than solid P25, in an aqueous phase. Therefore, it could be reasonably supposed that, if these two factors can be taken into account designing graphene-TiO₂ nanocomposites, the much more efficient graphene-TiO₂ photocatalyst could be obtained toward numerous potential applications.

CONCLUSIONS

In summary, we have synthesized the GR-TiO₂ nanocomposites by interfacially engineering the unique 2D mat of GR by a facile two-step wet-chemistry approach. This preparation approach is able to sufficiently use the "structure-directing" role of solution processable GO in an aqueous phase, thereby leading to the excellent interfacial

contact between TiO₂ and the GR surface. As a result, the as-synthesized GR-TiO₂ exhibits a much more active visible light photocatalytic activity than its analogue CNT-TiO₂ and that prepared by a simply random integration of TiO₂ and GR sheet toward selective oxidation of alcohols to aldehydes using dioxygen as oxidant under mild conditions. This study clearly signifies that more efficient GR-semiconductor photocatalysts can be developed through rational design and engineering the GR surface with semiconductor ingredients.

Importantly, our work is the first time to conceptually demonstrate how to synthesize a more efficient GR-semiconductor photocatalyst and the key importance of preparative methods on affecting the morphology of as-prepared GR-semiconductor nanocomposites and their photocatalytic activity. Furthermore, a comparison study between GR-semiconductor and CNT-semiconductor as photocatalyst is inevitably required, which will promote our in-depth fundamental understanding on the analogy and difference between GR and CNT on controlling the morphology of GR (or CNT)-semiconductor nanocomposites and enhancing the photocatalytic performance of semiconductor. Unfortunately, such a comparison is often neglected so far.^{12–21} Therefore, we herein appeal the photocatalysis community to pay attention to this respect rather than separately imposing hype on the miracle of GR in much the same way as its carbon forebears,^{31,32} which could significantly and ultimately advance our rational fabrication of smart graphene-semiconductor nanocomposites for artificial photosynthesis. Finally, it is hoped that our current research work could open a new doorway to exploit graphene-semiconductor composite materials in the field of photocatalytic selective organic synthesis, which would further enrich the potential applications related to graphene's world.

METHODS

Catalyst Preparation. Fabrication of graphene(GR)-TiO₂ nanocomposites: (a) graphene oxide(GO) was synthesized by the modified Hummers' method (Supporting Information);^{43–46} (b) synthesis of GR-TiO₂ nanocomposites: GO was dispersed into 200 mL of deionized water solution completely by ultrasonication, and then 4.0 g of TiF₄ was added to the given amount of the above GO solution to prepare GO-TiO₂ nanocomposites with different weight addition ratios of GO. The resulting solution was ultrasonicated for 1 h and then heated to 333 K in an oil-bath kept with magnetic stirring for 24 h. The mixture was then filtered, washed until the pH of rinsewater became neutral, and fully dried at 333 K in oven to get the GO-TiO₂ nanocomposites. Then, GO-TiO₂ was aged in a 26 mL of deionized water and 13 mL of anhydrous ethanol solution with vigorous stirring for 0.5 h to obtain a homogeneous suspension. After that, it was transferred to 50 mL Teflon-sealed autoclave and maintained at 393 K for 12 h. Subsequently, the products were cooled to room temperature and recovered by filtration, washed by water, and fully dried at 333 K in oven to get the final GR-TiO₂ nanocomposites with different weight addition ratios of GR, namely 1, 5,

10, 30, and 50% GR-TiO₂. CNTs used herein were multiwalled CNTs (no. L-MWNT-60100, diameter 60–100 nm, length 5–15 μm, purity 95–98%), which are supplied from Shenzhen Nanotech Port Co., Ltd., China. For CNT-TiO₂ nanocomposites, the synthesis procedures are similar except that GO is replaced by the acid-washed CNT that is well dispersed in water.

Catalyst Characterization. The X-ray diffraction (XRD) patterns of the samples were collected on a Bruker D8 Advance X-ray diffractometer with Cu Kα radiation. The accelerating voltage and the applied current were 40 kV and 40 mA, respectively. The optical properties of the samples were analyzed by UV-vis diffuse reflectance spectroscopy (UV-vis DRS) using a UV-vis spectrophotometer (Cary-500, Varian Co.), in which BaSO₄ was used as the background. The Brunauer-Emmett-Teller (BET) specific surface area (*S*_{BET}) of the samples was analyzed by nitrogen adsorption in a Micromeritics ASAP 2020 apparatus. SEM images were obtained by field emission scanning electron microscopy on a FEI Nova NANOSEM 230 spectrophotometer. TEM images were obtained using a JEOL model JEM 2010 EX instrument at an accelerating voltage of 200 kV. Raman spectroscopy was performed on a Renishaw Inva Raman System 1000 with a 532 nm Nd:YAG excitation source at room

temperature. X-ray photoelectron spectroscopy (XPS) measurements were performed using a Thermo Scientific ESCA Lab250 spectrometer which consists of a monochromatic Al K α as the X-ray source, a hemispherical analyzer and sample stage with multiaxial adjustability to obtain the composition on the surface of samples. Electron spin resonance (ESR) signal of the radicals spin trapped by 5,5-dimethyl-1-pyrroline-N-oxide (DMPO) was recorded on a Bruker EPR A300 spectrometer. The sample (5 mg) was dispersed in the solvent benzotrifluoride (BTF, 5 mL). Then, 25 μ L DMPO/benzyl alcohol solution (1:10, v/v) was added and oscillated to achieve the well-blending suspension. The settings for the ESR spectrometer were as follows: center field = 3507 G, microwave frequency = 9.84 GHz, and power = 6.36 mW. Photoelectrochemical measurements were performed in a homemade three electrode quartz cells with a PAR VMP3 Multi potentiostat apparatus. Pt plate was used as the counter, and Ag/AgCl electrode used as the reference electrodes, while the working electrode was prepared on fluoride-tin oxide (FTO) conductor glass. The sample powder (10 mg) was ultrasonicated in 1 mL of anhydrous ethanol to disperse it evenly to get a slurry. The slurry was spreading onto FTO glass whose side part was perviously protected using Scotch tape. The working electrode was dried overnight under ambient conditions. A copper wire was connected to the side part of the working electrode using a conductive tape. Uncoated parts of the electrode were isolated with epoxy resin. The electrolyte was 0.2 M of aqueous Na₂SO₄ solution without additive. The visible light irradiation source was a 300W Xe arc lamp system equipped with a UV cutoff filter ($\lambda > 400$ nm).

Catalyst Activity. Photocatalytic selective oxidation of alcohols was performed as follows: Typically, alcohol (0.1 mmol) and 8 mg catalyst were dissolved in the solvent of BTF (1.5 mL) saturated with pure molecular oxygen.^{29,39} This mixture was transferred into a 10 mL Pyrex glass bottle filled with molecular oxygen at a pressure of 0.1 MPa. The suspensions were irradiated by a 300 W Xe arc lamp with a UV-CUT filter ($\lambda > 400$ nm). After the reaction, the mixture was centrifuged to completely remove the catalyst particles. The remaining solution was analyzed with an Aglient gas chromatograph (GC-7820). Conversion, yield, and selectivity for selective oxidation of alcohols to target product aldehydes were defined as follows:

$$\text{conversion (\%)} = [(C_0 - C_t)/C_0] \times 100$$

$$\text{yield (\%)} = C_p/C_0 \times 100$$

$$\text{selectivity (\%)} = [C_p/(C_0 - C_t)] \times 100$$

where C_0 is the initial concentration of benzyl alcohol, and C_t and C_p are the concentration of reactant and product, respectively, during the photocatalytic reaction.

Acknowledgment. The support by the National Natural Science Foundation of China (20903022, 20903023, 21173045), the Award Program for Minjiang Scholar Professorship, Program for Changjiang Scholars and Innovative Research Team in Universities (PCSIRT0818), 973 Program (2007CB613306), and Program for Returned High-Level Overseas Chinese Scholars of Fujian province is gratefully acknowledged. We also cordially thank the valuable comments from reviewers to improve the quality of our research work.

Supporting Information Available: Photocatalytic activity of GR-P25 and CNT-P25 nanocomposites for selective oxidation of benzyl alcohol under visible light irradiation; photocatalytic activity of TiO₂-5% GR, TiO₂-5% CNT, P25-1% GR, and P25-1% CNT nanocomposites for selective oxidation of a range of benzylic alcohols and allylic alcohols under visible light irradiation; the plot of transformed Kubelka–Munk function versus the energy of light for TiO₂-GR and TiO₂-CNT nanocomposites; the XPS spectra of TiO₂-5% GO, TiO₂-5% GR, and TiO₂-5% GR after visible light irradiation in the reaction system; and experimental details for synthesis of graphene oxide. This material is available free of charge via the Internet at <http://pubs.acs.org>.

REFERENCES AND NOTES

- Geim, A. K. Graphene: Status and Prospects. *Science* **2009**, *324*, 1530–1534.
- Allen, M. J.; Tung, V. C.; Kaner, R. B. Honeycomb Carbon: A Review of Graphene. *Chem. Rev.* **2010**, *110*, 132–145.
- Rao, C. N. R.; Sood, A. K.; Subrahmanyam, K. S.; Govindaraj, A. Graphene: The New Two-Dimensional Nanomaterial. *Angew. Chem., Int. Ed.* **2009**, *48*, 7752–7777.
- Guo, S.; Dong, S. Graphene Nanosheet: Synthesis, Molecular Engineering, Thin Film, Hybrids, and Energy and Analytical Applications. *Chem. Soc. Rev.* **2011**, *40*, 2644–2672.
- Bai, H.; Li, C.; Shi, G. Functional Composite Materials Based on Chemically Converted Graphene. *Adv. Mater.* **2011**, *23*, 1089–1115.
- Kamat, P. V. Graphene-Based Nanoarchitectures. Anchoring Semiconductor and Metal Nanoparticles on a Two-Dimensional Carbon Support. *J. Phys. Chem. Lett.* **2010**, *1*, 520–527.
- Stankovich, S.; Dikin, D. A.; Dommett, G. H. B.; Kohlhaas, K. M.; Zimney, E. J.; Stach, E. A.; Piner, R. D.; Nguyen, S. T.; Ruoff, R. S. Graphene-Based Composite Materials. *Nature* **2006**, *442*, 282–286.
- Li, X. L.; Wang, X. R.; Zhang, L.; Lee, S. W.; Dai, H. J. Chemically Derived, Ultrasoft Graphene Nanoribbon Semiconductors. *Science* **2008**, *319*, 1229–1232.
- Compton, O. C.; Nguyen, S. T. Graphene Oxide, Highly Reduced Graphene Oxide, and Graphene: Versatile Building Blocks for Carbon-Based Materials. *Small* **2010**, *6*, 711–723.
- Wang, X.; Zhi, L. J.; Müllen, K. Conductive Graphene Electrodes for Dye-Sensitized Solar Cells. *Nano Lett.* **2008**, *8*, 323–327.
- Geim, A. K.; Novoselov, K. S. The Rise of Graphene. *Nat. Mater.* **2007**, *6*, 183–191.
- Zhang, Y.; Tang, Z. R.; Fu, X.; Xu, Y. J. TiO₂-Graphene Nanocomposites for Gas-Phase Photocatalytic Degradation of Volatile Aromatic Pollutant: Is TiO₂-Graphene Truly Different from Other TiO₂-Carbon Composite Materials? *ACS Nano* **2010**, *4*, 7303–7314.
- Zhang, H.; Lv, X. J.; Li, Y. M.; Wang, Y.; Li, J. H. P25-Graphene Composite as a High Performance Photocatalyst. *ACS Nano* **2010**, *4*, 380–386.
- Akhavan, O.; Ghaderi, E. Photocatalytic Reduction of Graphene Oxide Nanosheets on TiO₂ Thin Film for Photoinactivation of Bacteria in Solar Light Irradiation. *J. Phys. Chem. C* **2009**, *113*, 20214–20220.
- Zhang, X. Y.; Li, H. P.; Cui, X. L.; Lin, Y. Graphene/TiO₂ Nanocomposites: Synthesis, Characterization and Application in Hydrogen Evolution from Water Photocatalytic Splitting. *J. Mater. Chem.* **2010**, *20*, 2801–2086.
- Chen, C.; Cai, W.; Long, M.; Zhou, B.; Wu, Y.; Wu, D.; Feng, Y. Synthesis of Visible-Light Responsive Graphene Oxide/TiO₂ Composites with p/n Heterojunction. *ACS Nano* **2010**, *4*, 6425–6432.
- Zhou, K.; Zhu, Y.; Yang, X.; Jiang, X.; Li, C. Preparation of Graphene-TiO₂ Composites with Enhanced Photocatalytic Activity. *New J. Chem.* **2011**, *35*, 353–359.
- Zhang, Y.; Pan, C. TiO₂/Graphene Composite from Thermal Reaction of Graphene Oxide and Its Photocatalytic Activity in Visible Light. *J. Mater. Sci.* **2011**, *46*, 2622–2626.
- Fan, W.; Lai, Q.; Zhang, Q.; Wang, Y. Nanocomposites of TiO₂ and Reduced Graphene Oxide as Efficient Photocatalysts for Hydrogen Evolution. *J. Phys. Chem. C* **2011**, *115*, 10694–10701.
- Guo, J.; Zhu, S.; Chen, Z.; Li, Y.; Yu, Z.; Liu, Q.; Li, J.; Feng, C.; Zhang, D. Sonochemical Synthesis of TiO₂ Nanoparticles on Graphene for Use as Photocatalyst. *Ultrason. Sonochem.* **2011**, *18*, 1082–1090.
- Xu, T.; Zhang, L.; Cheng, H.; Zhu, Y. Significantly Enhanced Photocatalytic Performance of ZnO via Graphene Hybridization and the Mechanism Study. *Appl. Catal., B* **2011**, *101*, 382–387.
- Xu, Y. J.; Zhuang, Y. B.; Fu, X. Z. New Insight for Enhanced Photocatalytic Activity of TiO₂ by Doping Carbon Nanotubes: A Case Study on Degradation of Benzene and Methyl Orange. *J. Phys. Chem. C* **2010**, *114*, 2669–2676.

23. Woan, K.; Pyrgiotakis, G.; Sigmund, W. Photocatalytic Carbon-Nanotube-TiO₂ Composites. *Adv. Mater.* **2009**, *21*, 2233–2239.
24. Leary, R.; Westwood, A. Carbonaceous Nanomaterials for the Enhancement of TiO₂ Photocatalysis. *Carbon* **2011**, *49*, 741–772.
25. Yu, Y.; Yu, J. C.; Yu, J. G.; Kwok, Y. C.; Che, Y. K.; Zhao, J. C.; Ding, L.; Ge, W. K.; Wong, P. K. Enhancement of Photocatalytic Activity of Mesoporous TiO₂ by Using Carbon Nanotubes. *Appl. Catal., A* **2005**, *289*, 186–196.
26. Wang, W.; Serp, P.; Kalck, P.; Faria, J. L. Photocatalytic Degradation of Phenol on MWNT and Titania Composite Catalysts Prepared by a Modified Sol-Gel Method. *Appl. Catal., B* **2005**, *56*, 305–312.
27. Yao, Y.; Li, G. H.; Ciston, S.; Lueptow, R. M.; Gray, K. A. Photoreactive TiO₂/Carbon Nanotube Composites: Synthesis and Reactivity. *Environ. Sci. Technol.* **2008**, *42*, 4952–4957.
28. Enache, D. I.; Edwards, J. K.; Landon, P.; Solsona-Espriu, B.; Carley, A. F.; Herzing, A. A.; Watanabe, M.; Kiely, C. J.; Knight, D. W.; Hutchings, G. J. Solvent-Free Oxidation of Primary Alcohols to Aldehydes Using Au-Pd/TiO₂ Catalysts. *Science* **2006**, *311*, 362–365.
29. Zhang, M.; Chen, C. C.; Ma, W. H.; Zhao, J. C. Visible–Light–Induced Aerobic Oxidation of Alcohols in a Coupled Photocatalytic System of Dye–Sensitized TiO₂ and TEMPO. *Angew. Chem., Int. Ed.* **2008**, *47*, 9730–9733.
30. Hudlicky, M. *Oxidation in Organic Chemistry*; American Chemical Society: Washington, D.C., 1990.
31. Editorials, The Long Game. *Nature* **2011**, *473*, 419.
32. Noorden, R. V. The Trials of New Carbon. *Nature* **2011**, *469*, 14–16.
33. Fujishima, A.; Zhang, X.; Tyrk, D. A. TiO₂ Photocatalysis and Related Surface Phenomena. *Surf. Sci. Rep.* **2008**, *63*, 515–582.
34. Xu, H.; Wang, W.; Zhu, W. Shape Evolution and Size-Controllable Synthesis of Cu₂O Octahedra and Their Morphology-Dependent Photocatalytic Properties. *J. Phys. Chem. B* **2006**, *110*, 13829–13834.
35. Mao, Y.; Wong, S. S. Size- and Shape- Dependent Transformation of Nanosized Titanate into Analogous Anatase Titania Nanostructures. *J. Am. Chem. Soc.* **2006**, *128*, 8217–8226.
36. Bi, Y.; Ouyang, S.; Umezawa, N.; Cao, J.; Ye, J. Facet Effect of Single-Crystalline Ag₃PO₄ Sub-microcrystals on Photocatalytic Properties. *J. Am. Chem. Soc.* **2011**, *133*, 6490–6492.
37. Loh, K. P.; Bao, Q.; Eda, G.; Chhowalla, M. Graphene Oxide as a Chemically Tunable Platform for Optical Applications. *Nat. Chem.* **2010**, *2*, 1015–1024.
38. Jahan, M.; Bao, Q.; Yang, J. X.; Loh, K. P. Structure-Directing Role of Graphene in the Synthesis of Metal-Organic Framework Nanowire. *J. Am. Chem. Soc.* **2010**, *132*, 14487–14495.
39. Zhang, N.; Fu, X.; Xu, Y. J. A Facile and Green Approach to Synthesize Pt@CeO₂ Nanocomposite with Tunable Core-Shell and Yolk-Shell Structure and Its Application as a Visible Light Photocatalyst. *J. Mat. Chem.* **2011**, *21*, 8152–8158.
40. Liang, Y. T.; Vijayan, B. K.; Gray, K. A.; Hersam, M. C. Minimizing Graphene Defects Enhances Titania Nanocomposite-Based Photocatalytic Reduction of CO₂ for Improved Solar Fuel Production. *Nano Lett.* **2011**, *11*, 2865–2870.
41. Akhavan, O. Graphene Nanomesh by ZnO Nanorod Photocatalysts. *ACS Nano* **2010**, *4*, 4174–4180.
42. Akhavan, O.; Abdolohad, M.; Esfandiari, A.; Mohatashami-far, M. Photodegradation of Graphene Oxide Sheets by TiO₂ Nanoparticles after a Photocatalytic Reduction. *J. Phys. Chem. C* **2010**, *114*, 12955–12959.
43. Hummers, W. S.; Offeman, R. E. Preparation of Graphitic Oxide. *J. Am. Chem. Soc.* **1958**, *80*, 1339.
44. Kovtyukhova, N. I.; Ollivier, P. J.; Martin, B. R.; Mallouk, T. E.; Chizhik, S. A.; Buzaneva, E. V.; Gorchinskiy, A. D. Layer-by-Layer Assembly of Ultrathin Composite Films from Micron-Sized Graphite Oxide Sheets and Polycations. *Chem. Mater.* **1999**, *11*, 771–778.
45. Pan, D. Y.; Wang, S.; Zhao, B.; Wu, M. H.; Zhang, H. J.; Wang, Y.; Jiao, Z. Li Storage Properties of Disordered Graphene Nanosheets. *Chem. Mater.* **2009**, *21*, 3136–3142.
46. Cote, L. J.; Kim, F.; Huang, J. X. Langmuir-Blodgett Assembly of Graphite Oxide Single Layers. *J. Am. Chem. Soc.* **2009**, *131*, 1043–1049.